Atmospheric Boundary Layer as a Laboratory for Modeling Infrasound Propagation and Scattering in the Atmosphere

Igor Chunchuzov, Sergey Kulichkov, Oleg Popov, Vitaly Perepelkin, Aram Vardanyan & Gagik Ayvazyan

Pure and Applied Geophysics
pageoph

ISSN 0033-4553

Pure Appl. Geophys.
DOI 10.1007/s00024-020-02507-y

Springer

Pure Appl. Geophys.

https://doi.org/10.1007/s00024-020-02507-y

Pure and Applied Geophysics

Atmospheric Boundary Layer as a Laboratory for Modeling Infrasound Propagation and Scattering in the Atmosphere

Igor Chunchuzov,[1] Sergey Kulichkov,[1] Oleg Popov,[1] Vitaly Perepelkin,[1] Aram Vardanyan,[2] and Gagik Ayvazyan[2]

Abstract—In this work, we show that large-scale processes of the long-range propagation and scattering of infrasound signals in stratospheric and thermospheric waveguides are to some extent similar to the smaller scale processes of waveguide propagation and scattering of acoustic signals in stably stratified ABL. Moreover, we note a resemblance between the zeroth order tropospheric mode and the Lamb mode that is observed for larger nuclear explosions. The results of physical modeling of the long-range propagation of infrasound signals in the atmosphere by studying the propagation of the acoustic pulses from detonation sources in the stably stratified atmospheric boundary layer (ABL) are presented. Such modeling became possible due to continuous measurement of the wind velocity and temperature profiles in the ABL by Doppler sodar and temperature profiler, respectively. The resemblance between the propagation of the infrasound signals from surface explosions (20–70 t TNT) in the "shallow" tropospheric wave guide and propagation of Lamb mode from nuclear explosions is found. Also, the propagation of infrasound signals in the stratospheric wave guide is modeled by studying the propagation of acoustic pulses in the ABL during morning hours (after sunrise), when an effective sound speed profile in the ABL is similar to that in the stratospheric wave guide. The instantaneous vertical profiles of the effective sound speed and wind velocity fluctuations in the thin layers of the stably stratified ABL located at different heights (up to 700 m) above the ground and at different distances from the source (up to 2.25 km) have been retrieved using the wave forms and travel times of the recorded arrivals of the acoustic pulses from the detonation sources. The effect of scattering of acoustic pulses from the fine-scale layered structure of the stably stratified ABL is studied to model the effect of scattering of infrasound signals from the fine-scale layered structure of the stratosphere.

Keywords: fine-scale layered structure, scattering, detonation generator.

1. Introduction

In recent decades, it has become clear that the problem of infrasound monitoring of explosions cannot be solved without taking into account the influence of the atmospheric fine-scale layered wind velocity and temperature structure on the parameters of infrasonic signals such as propagation time, arrival azimuths, wave form, amplitude and duration.

The large-scale (as compared to the characteristic wave lengths of infrasound waves) wind and temperature inhomogeneities cause variations in the azimuth of infrasound propagation that lead to the error in localization of infrasound sources. The layered inhomogeneities of smaller scales, which are comparable to the wavelengths of infrasound waves, significantly scatter infrasound field so that this field penetrates to the zones of acoustic shadow and can be detected experimentally.

The information on large-scale wind and temperature fluctuations can be retrieved from ECMFW, G2S, or similar data sources (Drob et al. 2013) with some level of confidence (uncertainties are on the order of 10–20 m/s on wind speeds). However, the fluctuations of smaller scales are typically not included in such specifications.

At present, many works are devoted to the theoretical and experimental studies of the combined effect of stratification of mean wind speed and temperature, and their mesoscale fluctuations in the stratosphere, mesosphere, and lower thermosphere, on the long-range propagation and scattering of infrasound waves (Gibson et al. 2009; Le Pichon et al. 2010; Gainville et al. 2010; Drob et al. 2013; Hedlin and Walker 2013; Chunchuzov et al. 2015a,b;

[1] Obukhov Institute of Atmospheric Physics, 3 Pyzhevskii Per., 119017 Moscow, Russia. E-mail: igor.chunchuzov@gmail.com

[2] Barva Innovation Center, 0501 Talin, Armenia.

Published online: 20 May 2020

Lalande and Waxler 2016; Green et al. 2018; Damiens et al. 2018; Sabatini et al. 2019; Waxler and Assink 2019).. In recent decades, intensive theoretical and experimental studies of the propagation of acoustic pulses in near-surface waveguides formed in a stably-stratified atmospheric boundary layer (ABL) have also been carried out (Chunchuzov et al. 1990; 2010); (Waxler 2002; Waxler et al. 2008; Talmadge et al. 2008; Blom and Waxler 2012). In addition to the typical signal arrivals in the surface waveguides, the experimental studies also revealed arrivals caused by the signal scattering on the fine-scale layered structure of a stably stratified ABL (Chunchuzov et al. 2017, 2019). The effect of scattering of acoustic pulses in the ABL had some resemblance to the scattering of infrasound signals on a fine-scale layered structure in the stratosphere, since this effect resulted in the appearance of signals in the zones of acoustic shadow on the ground, predicted by the geometric acoustics.

The aim of this paper is to show, on the basis of the already known results of works mentioned above, that large-scale processes of the long-range propagation and scattering of infrasound signals in stratospheric waveguides are to some extent similar to the smaller scale processes of waveguiding propagation and scattering of acoustic signals in stably stratified ABL under formation of temperature inversion elevated above ground. The possibility of physical modeling of the long-range propagation of infrasound signals in the stratospheric and thermospheric wave guides was first justified in the works (Kulichkov et al. 2007; Chunchuzov et al. 2019).

In Sect. 2 of this paper we obtain an analytical solution that describes acoustic field from a point pulsed source in the Epstein layer over rigid boundary and study the evolution of the pulse waveform with decreasing effective thickness of this layer. In Sect. 3 we analyze acoustic pulse propagation in the "shallow" tropospheric wave guide with small effective thickness, and compare this process with the propagation in the atmosphere of the so-called Lamb mode generated by nuclear explosions. Contrary to the Sect. 3 we consider in Sect. 4 the case of "deep" wave guide with large effective thickness. The results of study of the propagation of acoustic pulses generated by detonation sources in the stably stratified ABL during morning hours (after sunrise) are presented. The specific case when the effective sound speed profile in the ABL resembles that in the stratospheric wave guide is analyzed using ray tracing method. The effect of scattering of acoustic pulses from a fine-scale layered structure of the stably stratified ABL is studied in Sect. 5. Its resemblance with the effect of scattering of the infrasound signals from the fine-scale layered structure of the upper atmosphere is discussed.

2. *Modeling Acoustic Pulse Propagation in the Wave Guides*

When modeling sound propagation in the atmospheric wave guides we deal with the atmospheric layers having vertical profiles of the effective sound speed $C_{eff}(z)$ (sound speed plus wind velocity projection on the direction of wave propagation) described by the same dimensionless function of the normalized height z over ground ($z = 0$):

$$C_{eff}(z)/C_{eff}(z=0) = F(z/h), \tag{1}$$

where h is the vertical scale of the inhomogeneous atmospheric layer. The validity of the effective sound speed approximation in moving media was discussed, particularly, by Godin et al. (1993), Ostashev and Wilson (2015). One example of moving inhomogeneous layer is so-called Epstein layer (Fig. 1) with the following vertical profiles of wind speed

$$V(z) = V_0 \cdot \left[1 - \cosh^{-2}\left(\frac{z}{2h}\right)\right], \tag{2}$$

and temperature

$$T(z) = T_0 \cdot \left\{1 + \Delta \cdot \left[1 - \cosh^{-2}\left(\frac{z}{2h}\right)\right]\right\}, \tag{3}$$

where $V_0 \equiv V(z \to \infty)$, $T_0 \equiv T(z=0)$, and $\Delta \equiv |T(z \to \infty) - T_0|/T_0 << 1$ is the relative vertical jump in temperature within the layer. The effective sound speed profile $C_{eff}(z)$ $C_{eff}(z) = \vec{V}\vec{n} + c \approx V\cos(\varphi) + c + O(V^2/c^2)$ for the Epstein layer is shown in Fig. 1, where $c = \sqrt{\gamma RT}$ is the sound speed, R is gas constant, $\gamma = c_p/c_v$ is the ratio of heat capacities of air at constant pressure and volume, $\vec{n}$ is the normal to the wave front of acoustic wave, φ is the azimuth of the reception point with respect to the

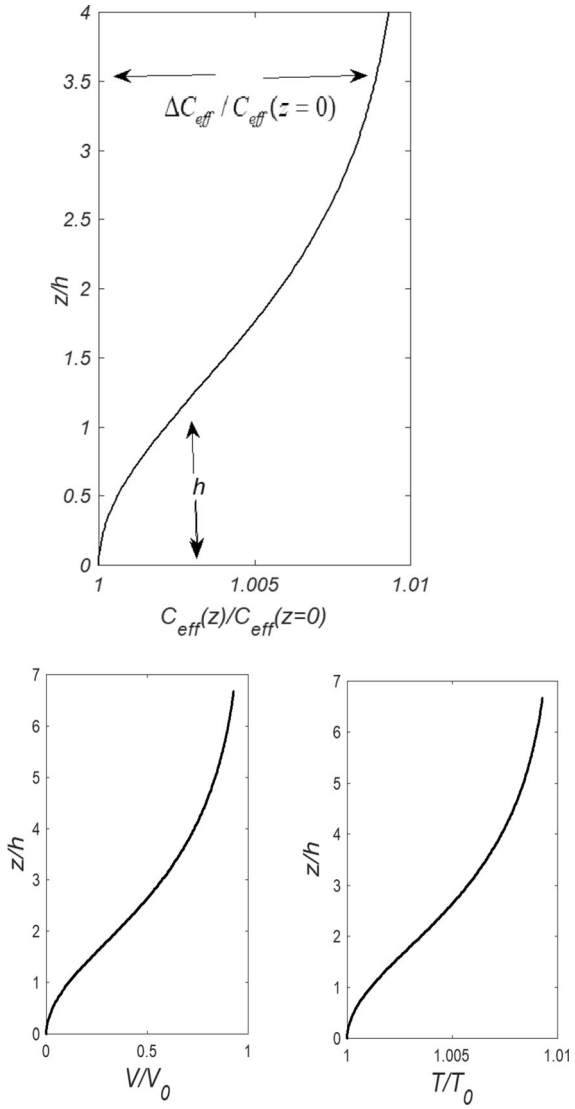

Figure 1
Epstein layer. Vertical profiles of the normalized effective sound speed $Ceff\,(z)$ (top), wind speed V(z) and temperature T(z) (bottom)

direction $\varphi = 0$ of the wind velocity vector $\vec{V}$ (it was assumed that the difference between directions of $\vec{n}$ and φ is a small value of order Mach number $V/c << 1$), and $\Delta C_{eff} = \left|C_{eff}(z \to \infty) - C_{eff}\ (z = 0)\right|$ is the vertical jump in $C_{eff}(z)$ within the layer.

If $\Delta C_{eff} > 0$, then the Epstein layer serves as a waveguide for acoustic waves. Moreover, it is possible to obtain an analytic solution of the Helmholtz equation with the boundary conditions on the rigid boundary and at the infinity to present acoustic field at a distance r from a point pulsed source as a superposition of acoustic wave modes p_n, $n = 0, 1, 2,\ldots$, the field of each of them has the form

$$p_n \approx \frac{2R_0}{r}\left[\left|\tilde{P}(R_0,\omega)G_n(\omega,\varphi,z,z_0)\right|\right]_0 \cos[\xi_n r - \omega_n t + \pi/2 + \arg G_n + \arg \tilde{P}]_0, \tag{4}$$

where $\tilde{P}(R_0,\omega)$ is a frequency spectrum of the generated pulse wave form at short distance R_0 from the source, and $G_n(\omega,\varphi,z,z_0)$ is the transfer function of the wave guide. In the particular case, when the source and receiver are in the vicinity of the rigid ground surface ($z = z_0 = 0$), both the amplitude and phase terms in expression (4) for the wave field take the following forms (Chunchuzov et al. 1990):

$$|G_n(\omega,\varphi,z=0,z_0=0)|_0 = 2\tilde{\omega}\cdot \left(\frac{\omega_n^0}{\omega_n} - 1\right)\left[1 - \left(1 - \frac{\omega_n}{\omega_n^0}\right)^2\right]^{-1/2}, \tag{5}$$

$$[\omega_n t - \xi_n r]_0 \equiv \Phi_n(\tau) = \omega_n^0\left[\tau - \tau_m\left(1 - \frac{\omega_n}{\omega_n^0}\right)^2\right], \tag{6}$$

where $\tilde{\omega} = \frac{2c_0}{\varepsilon_0^{1/2}h}$, $\omega_n = \frac{c_0}{\varepsilon_0^{1/2}h}(2n + 1/2)$ is the waveguide eigenfrequency of the order n, $c_0 \equiv C_{eff}(z = 0)$, $\varepsilon_0 = 2\Delta C_{eff}/C_{eff}(z = 0)$ is the relative jump in effective sound speed (doubled), $\tau = t - r/c_\infty$ is the running time measured from the moment $t_0 = r/c_\infty$, where $C_{eff}(z \to \infty) \equiv c_\infty = [c(z) + V(z)\cos(\varphi)]_{z\to\infty}$ is the effective sound speed in the azimuthal direction φ at $z \to \infty$, and $\tau_m = \frac{r}{c_0} - \frac{r}{c_\infty} \approx \frac{\varepsilon_0 r}{2c_\infty} = \frac{\varepsilon_0 t_0}{2}$ is the time interval limiting the total duration of the signal arriving at the receiving point at distance r from the source,

$$\omega_n^0(\tau) = \omega_n \Big/ \left(1 - \frac{2\tau}{\varepsilon_0 t_0}\right)^{1/2}, \tag{7}$$

is the local mode frequency within interval $0 \le \tau \le \varepsilon_0 t_0/2$.

Let the emitted pulse of acoustic pressure in the vicinity of its source be given in the form

$$p'(R_0,t) = -P_m \frac{t}{\tau_0}\exp\left[\frac{1}{2}\left(1 - \frac{t^2}{\tau_0^2}\right)\right], \tag{8}$$

where P_m is maximum pressure at distance $R_0 \sim c_0\tau_0$, and τ_0 is the characteristic duration of the

positive (or negative) phase of a bipolar pulse. Substitute the Fourier spectrum corresponding to this pulse

$$\tilde{P}_0(R_0,\omega) = (2\pi)^{-1/2} e^{-i\pi/2} \cdot P_m \cdot \omega\tau_0^2 \cdot \exp[(1 - \omega^2\tau_0^2)/2], \quad (9)$$

into expression (4) for the pulse field. Note that at $n > > 1$ the waveguide eigenfrequencies are located equidistantly, $\omega_n \approx \tilde{\omega} \cdot n$, with interval $\tilde{\omega}$ between neighboring modes. If this is taken into account, the effective waveguide thickness at frequency $\omega_m = \tau_0^{-1}$ corresponding to the maximum amplitude pulse spectrum may be written in the form:

$$M_0(\omega = \omega_m) \equiv M_m = 2\varepsilon_0^{1/2}\omega_m h/c_0 = 4\omega_m/\tilde{\omega}. \quad (10)$$

The effective waveguide thickness (10) characterizes the number of waveguide eigenfrequencies ω_n that are within the frequency band of the spectrum (9) (with bandwidth $4\omega_m$). With Eq. (10) taken into account, the local mode frequencies may be written as

$$\omega_n^0 \approx \tilde{\omega} n \Big/ \left(1 - \frac{\tau}{\tau_m}\right)^{1/2} = \frac{4\omega_m}{M_m} n \Big/ \left[1 - \frac{\omega_m \tau}{2\pi r/L_i}\right]^{1/2}, \quad (n > > 1), \quad (11)$$

where

$$L_i \equiv 2\pi|\xi_n - \xi_{n'}|^{-1} \approx 2\pi \frac{2c_\infty}{\varepsilon_0 \omega_m}, \quad (12)$$

is the minimum spatial period of mode interference (Brekhovskikh and Lysanov 2003, Sect. 6.7) at frequency ω_m, which is inversely proportional to the maximum difference between the wavenumbers $|\xi_n - \xi_{n'}| = \frac{\omega_m}{c_0}|\cos\chi_n - \cos\chi_{n'}|$, where χ_n is the maximum grazing angle of acoustic modes ($\sin\chi_n \approx \varepsilon_0^{1/2}$), which corresponds to the maximum vertical angle of the ray path trapped by the waveguide, and $\chi_{n'}$ is the minimum grazing angle of modes (for the source on the ground surface $\chi_{n'} \approx 0$).

Substituting expressions (5), (6), (9)–(11) into (4), and taking into account that $\omega_m\tau_m = \omega_m\varepsilon_0 r/(2c_\infty) = 2\pi r/L_i$ and $\tilde{\omega}\tau_0 = 4\omega_m\tau_0 M_m^{-1} = 4M_m^{-1}$, one can find that, for the given number n, the mode amplitude $\left|\tilde{P}(R_0,\omega_n^0)G_n(\omega_n^0,\varphi,z=0,z_0=0)\right|P_m^{-1}$ normalized to the initial-pulse amplitude P_m, and the phase of mode (6) ($\arg\tilde{P}_0 = -\pi/2$ and $\arg G_n = 0$) depend only on the effective waveguide thickness M_m, dimensionless time $\omega_m\tau$, and dimensionless distance r/L_i. Summation of modes leads to the fact that the normalized pulse field (4) is also the function of dimensionless variables M_m, $\omega_m\tau$, and r/L_i:

$$\frac{p'(r,\varphi,z=0,t)\cdot r}{P_m R_0} = \Pi\left(M_m, \frac{r}{L_i}, \omega_m\tau\right). \quad (13)$$

The same conclusion is also valid for the exponential layer also analyzed by Chunchuzov et al. (1990). The exponential layer can be obtained from Epstein layer by replacement $\cosh^{-2}(\frac{z}{2h})$ on $exp(-\frac{z}{h})$ in formulas (2) and (3).

If the source and receiver are not on the ground surface, the pulse field (13) will additionally depend on dimensionless heights of the receiver and source, $\frac{z}{h}$ and $\frac{z_0}{h}$.

The solution (4)–(9) obtained by Chunchuzov et al. (1990) is given here to show that the waveform at a certain dimensionless distance from the source [defined by dimensionless function (13)] depends only on the effective waveguide thickness (10). In other words, if different pulsed sources (for example, explosions and detonation generators) generate identical signals in their wave forms, but differing in duration τ_0, then the waveforms (13) of their signals at some dimensionless distance r/L_i from the source will be similar in waveguides with the same effective thickness $M_m = 2\varepsilon_0^{1/2}h/c_0\tau_0$, although vertical scales h and relative jumps in effective sound speed, $\varepsilon_0 = 2\Delta C_{eff}/C_{eff}(z=0)$ may be different.

Figure 2 shows the evolution of signal waveform in the Epstein layer above the rigid boundary at a distance of 4 km from the source ($z_0 = z = 0$), when the effective waveguide thickness M_m decreases from 15.78 to 3.95 (on the left). Particularly, the decrease in M_m (or in the number n of propagating modes) and change in the waveform of the signal can be due to an increase of the azimuth φ relative to the wind velocity direction $\varphi = 0$. On the right in Fig. 2 are shown corresponding normalized modes $\frac{p_n}{P_m}\frac{r}{R_0}$ of different orders $n = 0, 1, 2,\ldots$, whose interference shapes the given signal. It is important to note that the wave forms of the signal with the same central frequency $f_m = 32$ Hz in Fig. 2b are the same for the

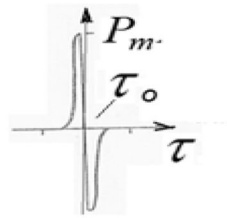

Initial signal

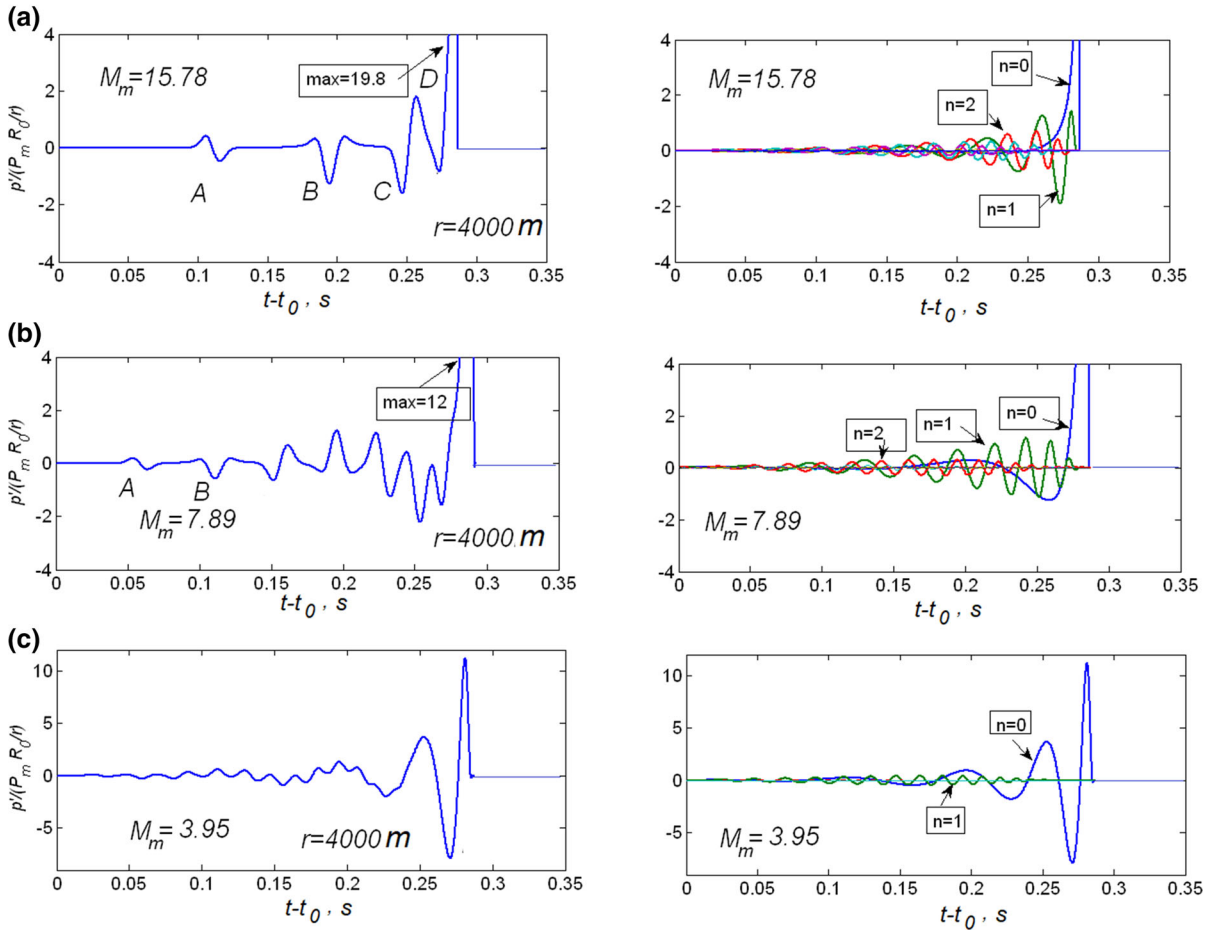

Figure 2

Initial signal near point source at r = R_0 (top) with the frequency $\omega_m = \tau_0^{-1}$ corresponding to the maximum of its frequency spectrum, and evolution of signal waveform in the Epstein layer above the rigid boundary at a distance r = 4 km from the source ($z_0 = z = 0$), while the effective waveguide thickness M_m decreases from 15.78 to 3.95 (on the left). On the right, corresponding normalized normal waves $\frac{p_n}{P_m}\frac{r}{R_0}$ of different orders n = 0, 1, 2, …, whose interference shapes the given signal. **a** M_m = 15.78, ($\varphi = 0, f_m = 1/(2\pi\tau_0) \approx$ 32 Hz. $\varepsilon_0 = 0.05$, h = 60 m, c_0 = 340 m/s); **b** M_m = 7.89, (f_m = 32 Hz, $\varepsilon_0 = 0.05$, h = 30 m, c_0 = 340 m/s) or (f_m = 32 Hz, $\varepsilon_0 = 0.0125$, h = 60 m, c_0 = 340 m/s); c) M_m = 3.95, ($\varphi = 0, f_m$ = 32 Hz, $\varepsilon_0 = 0.05$, h = 15 m, c_0 = 340 m/s)

Epstein layer (1)–(3) with different two sets of parameters: $\varepsilon_0 = 0.05$, h = 30 m and $\varepsilon_0 = 0.0125$, h = 60 m, but for the same effective thickness M_m = 7.89.

3. "Shallow" Wave Guide ($M_m << 1$)

When the effective thickness of the wave guide becomes small,$M_m << 1$, there is only one fundamental normal wave with $n = 0$ that propagates in the wave guide. In this case the modal wave number has a slightly nonlinear (cubic) dependence on frequency ($\sim \omega^3$)

$$\xi_0(\omega) \approx \omega/c_\infty (1 + \alpha \cdot \omega^2),\ \alpha \equiv \frac{\varepsilon_0^2 h^2}{2c_\infty^2}. \qquad (14)$$

It was shown by Chunchuzov (1986) that in such a "shallow" wave guide the evolution of the pulse wave form with increasing distance r from the point source is described by Korteweg-de Vries (KdV) equation (Karpman 1974):

$$\frac{\partial U}{\partial r} - \frac{\overline{\varepsilon} p_0'}{\overline{\rho} c_\infty^3} \frac{r_0^{1/2}}{r^{1/2}} U \frac{\partial U}{\partial \tau} - \frac{\alpha}{\infty} \frac{\partial^3 U}{\partial \tau^3} = 0, \qquad (15)$$

where $U = \frac{p'}{p_0'} \left(\frac{r}{r_0} \frac{\overline{\rho}(0)}{\overline{\rho}}\right)^{1/2}$, p_0' is acoustic pressure amplitude at a horizontal distance $r = r_0 \sim c_0 \tau_0$ from the point source, $\overline{\rho}$ is static density of the atmosphere, $\overline{\varepsilon} = (\gamma + 1)/2$, $\gamma = c_p/c_v$. The Eq. (15) takes into account both the nonlinearity of propagation and the cylindrical divergence of the field with increasing distance r from the source (Ko and Kuehl 1979; Pelinovskii 1982; Pelinovskii et al. 1984; Dorfman et al. 1981).

When increasing the power of the surface explosions the duration of the generated infrasound signals increases so that their frequency $f_m = \omega_m/(2\pi)$ corresponding to the maximum of the spectrum decreases [see, for example, the spectrum described by Eq. (9)]. The evolution of the form of the pulse specified at a distance of 1 km from the source ($f_m = \omega_m/(2\pi)$ = 0.8 Hz) with increasing distance r is shown in Fig. 3 (Chunchuzov 1986), where the parameters of the exponential $C_{eff}(z)$-profile in the lower tropospheric layer are:$\varepsilon_0 \approx 1.6 \cdot 10^{-2}$, h = 150 m, c_0 = 340 m/s, $M_m \sim 0.5$. The

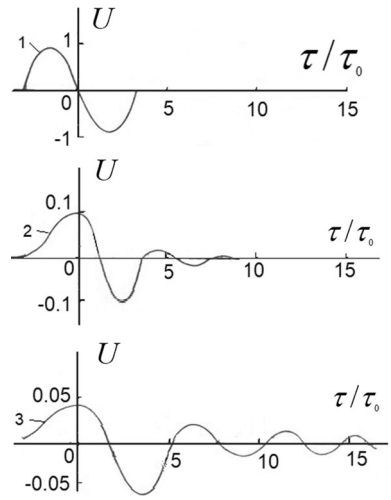

Figure 3
Evolution in the pulse form $U = \frac{p'}{p_0'} \left(\frac{r}{r_0} \frac{\overline{\rho}(0)}{\overline{\rho}}\right)^{1/2}$ on the ground surface ($z = 0$) with increasing distance r from the point source, where $\tau = t - r/c_\infty$, $\tau_0 = \omega_m^{-1}$ is the characteristic duration inversely proportional to (circular) frequency of the maximum of temporal spectrum of initial pulse: 1-an initial pulse specified at distance r_0 = 1 km from the source; 2- signal at distance ~ 45 km; and 3- signal at distance 140 km from the source

tropospheric arrivals of signals from 20 to 70 t of TNT surface explosions (Kulichkov 1992) propagating in tropospheric waveguides often had forms predicted by the KdV equation (Fig. 3) and consisted of the so-called Airy wave (the head part of the signals) and an oscillating tail.

It is interesting to note that the so-called Lamb mode, recorded at distances of tens of thousands of kilometers from a nuclear explosion, also has a similar shape (Pierce and Posey 1971; Kulichkov 1987). Actually, such a resemblance in the wave forms of the predicted tropospheric arrivals from 20 to 70 t of TNT surface explosions (Fig. 3) and those of Lamb modes from nuclear explosions (Fig. 4b) is not surprising since the latter is also described by the solution of KdV equation (Pierce and Posey 1971). Some difference between the calculated signals in Figs. 3 and 4b is likely caused by the fact, that they correspond to different ranges (normalized by the corresponding dispersion lengths) from the sources, although they have the same dispersion equation of the form (14).

Both the Lamb mode and low-order acoustic mode in the shallow tropospheric wave guide have a common dispersion relation along with surface waves

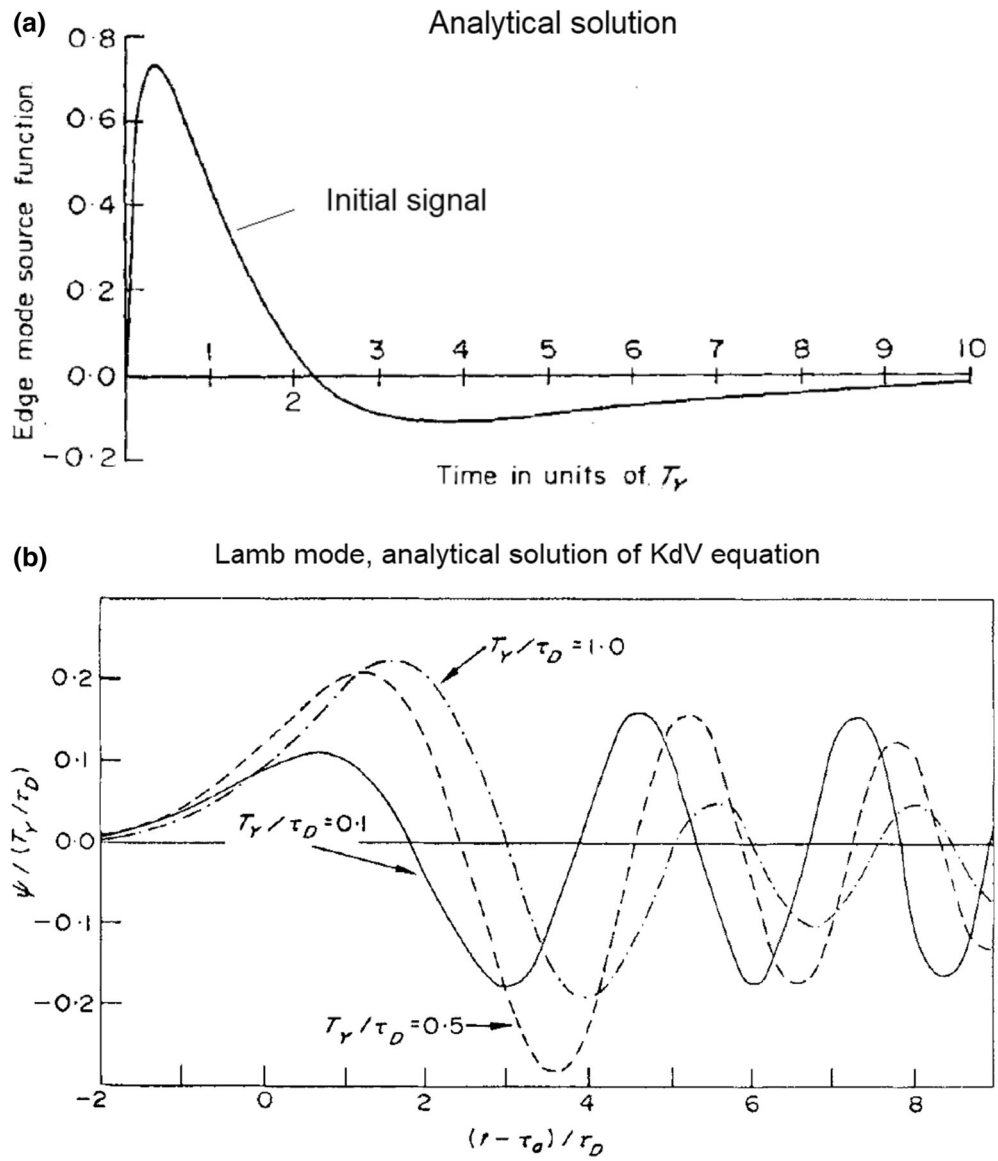

Figure 4
(reproduced from (Pierce and Posey 1971)). Analytical solution of the linearized KdV equation describing wave forms of the Lamb edge mode. **a** Initial wave form of the signal close to the source, T_γ is a characteristic time for the explosion. **b** Waveform factor Ψ(divided by T_γ/τ_D) with time t(relative to characteristic arrival time τ_a and in units of τ_D) for three values of the ratio T_γ/τ_D of characteristic source time T_γ to characteristic dispersion time τ_D

in shallow sea and other wave systems considered by Karpman. (1974), Zakharov et al. (1980), Pelinovskii (1982), Pelinovskii et al. (1984). The agreement of the wave forms predicted theoretically is confirmed by the comparison of the observed wave forms for the Lamb mode (Fig. 5, top) generated by nuclear explosion (10 Megaton TNT at Berkeley California, October 30 1962) (Pierce and Posey 1971), and tropospheric arrival (Fig. 5, bottom) from the 30 t TNT surface explosion that was recorded on April 14 1991 at a distance $r = 310$ km from the source during destruction of medium-range missiles in Russia (Kulichkov 1992).

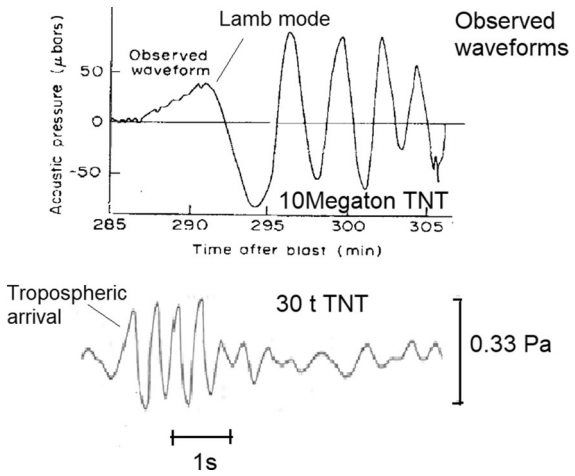

Figure 5
Observed waveforms for the Lamb mode (top, reproduced from (Pierce and Posey 1971)) generated by nuclear explosion (10 Megaton TNT at Berkeley California, October 30 1962), and tropospheric arrival from the 30 t TNT surface explosion recorded on April 14 1991 at a distance r = 310 km during destruction of medium- range missiles in Russia (bottom)

Thus, we found that there is a possibility for physical modeling the evolution of the wave form and duration of Lamb mode from nuclear explosion with increasing distance from the source by experimental studying of the propagation of the signal from surface explosions of medium power (20–70 t TNT) in the tropospheric wave guide. Such modeling is of great practical importance for estimating the power of nuclear explosion, which is rare event, by measuring certain changes in duration and amplitude of the Lamb mode with increasing distance r (Pierce and Posey 1971).

4. *Study of the Propagation of Acoustic Pulses from Detonation Sources in Stably Stratified ABL*

Contrary to the case of acoustic pulse propagation in the "shallow" ($M_m << 1$) wave guide (Sect. 3), we will consider now its propagation in the "deep' wave guides with high effective thickness ($M_m > > 1$). To study the propagation of acoustic pulses of stable wave form and duration in the tropospheric wave guide we used man-made pulsed sources shown in Fig. 6. In stably stratified ABL we can measure the

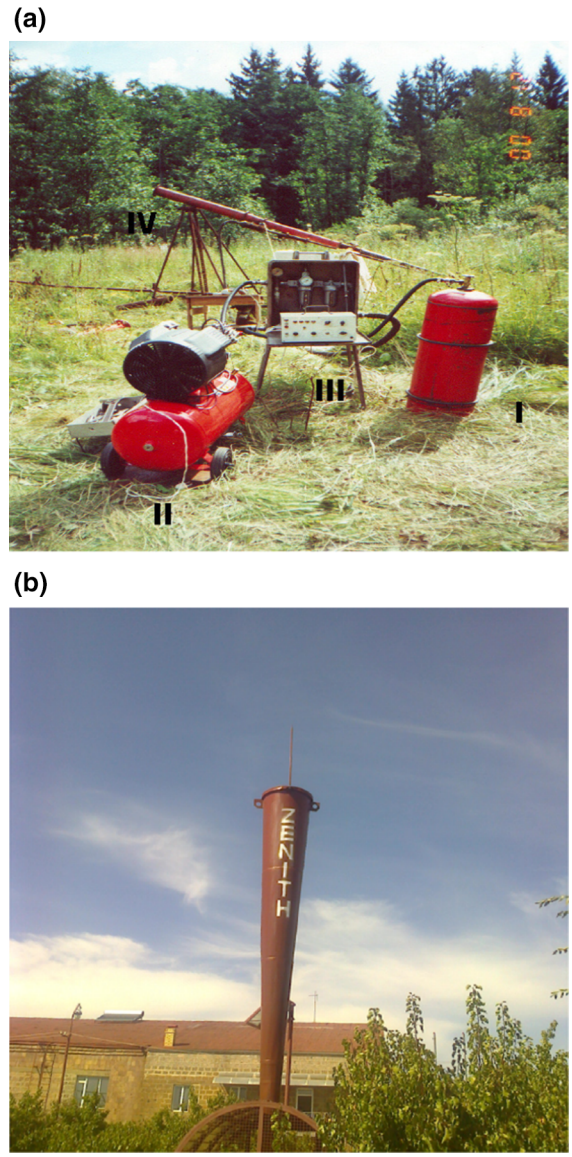

Figure 6
Detonation generator of acoustic pulses used for probing atmospheric boundary layer near Zvenigorod (**a**) and anti-hail acoustic cannon in Talin, Armenia (**b**)

vertical profile of wind (by using Doppler sodar) and temperature (using temperature profiler). This allows to estimate effective thickness of the wave guide M_m by approximating real wind and temperature profiles in the surface atmospheric layer with the analytical profiles (exponential, Epstein or linear profile) and study the dependence of the wave form predicted by Eq. (13) on the normalized distance $\frac{r}{L_i}$ and M_m along

different azimuths φ relative to the mean wind direction.

When the effective thickness of the waveguide becomes large ($M_m >> 1$) along with the number of modes propagating in the waveguide ($n >> 1$), then a transition from the wave theory to the ray approximation is possible (Brekhovskikh and Lysanov 2003). In this approximation, it is also possible to model the propagation of infrasound waves from explosions in the stratospheric and thermospheric waveguides by studying experimentally the propagation of acoustic pulses generated by detonation generator in a stably stratified ABL.

The vertical profiles of the effective sound speed *Ceff*, and the corresponding ray paths in the atmosphere obtained from rocket sounding data during conducting a series of surface explosions in Russia with a power of 20–70 t TNT (October 1990), and the ray paths for the acoustic pulses from the detonation generator calculated for the ABL during morning hours of July 12. 2005, are shown in Fig. 7.

In the direction of wind velocity in the stratosphere, a stratospheric waveguide is formed for infrasound waves from explosions, while in the opposite direction, where *Ceff* at stratopause heights $z \sim 40$ km less than at the ground surface, an acoustic shadow zone is formed for stratospheric reflections (Fig. 7, left). As for the total internal reflections of the infrasound waves from the lower thermosphere (altitudes of 100–130 km), they occur in any direction from the source.

The propagation of the infrasound signals in the stratospheric wave guide is well modeled by studying the propagation of acoustic pulses from the detonation generator in the ABL early in the morning hours after sunrise (Fig. 7. right). The convection under the nocturnal temperature inversion in the surface atmospheric layer, that arises after the sunrise, leads to the decrease of temperature and *Ceff* with increasing height z from the ground ($z = 0$) to $z = 100$ m, and then *Ceff* increases with z from 100 to 200 m within the elevated inversion layer. Such a *Ceff*- profile resembles a *Ceff*-profile in the stratospheric wave guide with the "stratopause" at height z $\sim$ 200 m. The corresponding ray paths in the ABL from the detonation source (Fig. 7 right) resemble the refraction of infrasound in the stratospheric wave guide

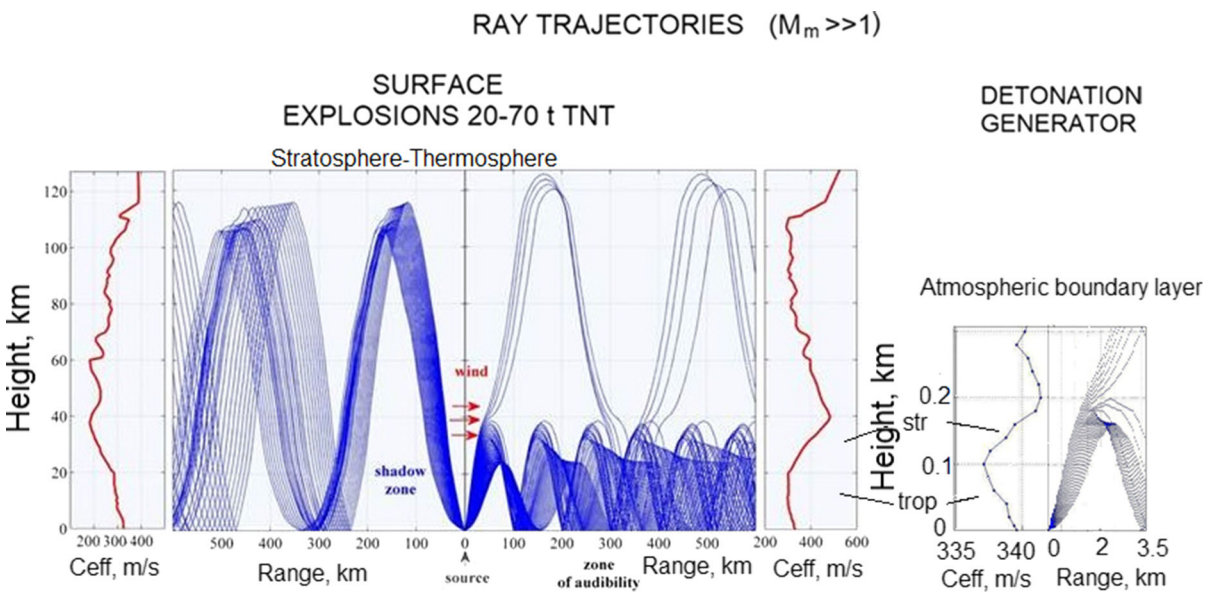

Figure 7

The vertical profiles of the effective sound speed $C_{eff}(z)$ and the corresponding ray paths in the atmosphere (left) obtained in October 20, 1990 from rocket sounding data during conducting a series of surface explosions in Russia with a power of 20–70 t TNT, and the ray paths (right). in the atmospheric boundary layer (ABL) calculated for the $C_{eff}(z)$-profile obtained on July 11–12, 2005 from Doppler sodar and temperature profiler measurements near Zvenigorod

(Fig. 7, left) and the appearance of the zones of shadow and audibility.

The similarity parameter $M_m = 2\varepsilon_0^{1/2}\omega_m h/c_0$ was introduced in Sect. 1 for the Epstein profile with one vertical scale h. For the case of a stratospheric waveguide with a maximum of $C_{eff}(z)$ near the stratopause ($z \sim 45$ to 55 km), exceeding the value of $C_{eff}(z)$ near ground surface, the profile of $C_{eff}(z)$ was also approximated by the Epstein profile in (Kulichkov et al. 1986). With such an approximation, the minimum of the temperature profile (3) and $C_{eff}(z)$ was not at $z = 0$, as in the case considered in Sect. 2, but approximately at the height z of the tropopause (10–15 km), and the point source was located at $z < 0$. In this case, it is easy to estimate the effective thickness (10) of the stratospheric waveguide for the signal from explosion with a frequency $\omega_m/2\pi \sim 0.6$ Hz. Taking the scale $h \sim 20$–25 km (which is approximately ½ the height of the stratopause), and the relative jump $\varepsilon_0 = 2\Delta C_{eff}/C_{eff} \sim 0.15$ for the profile $C_{eff}(z)$ between its minimum at the height of the tropopause, and its maximum at the height of the stratopause, we obtain that M_m is in the range 190–230. For such high values of M_m, we can use the ray approximation and compare the ray paths in the stratospheric waveguide in the wind direction (in Fig. 7 left) with the ray paths calculated for a similar profile $C_{eff}(z)$ in the ABL (shown in Fig. 7 right).

The central frequency of the spectra of pulses from the detonation generator is $\omega_m/2\pi \sim 60$ Hz, i.e. two orders of value higher than for signals from the explosion mentioned above. For the $C_{eff}(z)$-profile in the ABL the scale $h \sim 100$ m, $\varepsilon_0 \sim 0.04$, therefore $M_m \sim 44$. Thus, the ray approximation is also applicable for the ABL with $M_m \sim 44$ despite the fact that this value is 4–5 times lower than that for the stratospheric waveguide.

The ray trajectories in the ABL in Fig. 7 (right) resemble those in a stratospheric waveguide in the prevailing wind direction (Fig. 7 left). Such a resemblance suggests the possibility of modeling the propagation of infrasound signals in a stratospheric waveguide by studying the propagation of signals from a high-frequency acoustic sources in a small-scale surface waveguide in the ABL (compared with the stratospheric waveguide), formed in the periods of existence of the temperature inversion elevated above ground. This conclusion directly confirms the theoretical conclusion of Sect. 2 on the resemblance of the propagation of acoustic pulses of different durations in Epstein layers with different scales of h, but with close values of M_m.

5. *Modeling of the Effect of Atmospheric Gravity Wave Perturbations and Coherent Structures in the Atmosphere on Long-Range Infrasound Propagation*

In recent decades, the infrasound community of scientists has realized that the internal gravity waves (IGWs) and vortex structures existing in stably-stratified atmospheric layers have a significant effect on the long-range propagation of infrasound waves. (Chunchuzov 2004; Drob et al. 2013; Chunchuzov et al. 2015a, b; Lalande and Waxler 2016; Green et al. 2018; Waxler and Assink 2019; Millet et al. 2019). The anisotropic perturbations in wind and temperature fields induced by IGWs and vortex structures exist in the stratosphere, mesosphere, lower thermosphere and the stably-stratified ABL. The characteristic vertical scales of such perturbations grow with height due to a decrease in density of the atmosphere (see, for instance, Fritts and Alexander 2003), therefore it is possible to study the effects of scattering of infrasound from the fine-scale layered structure of the upper atmosphere by studying the effect of scattering of high-frequency acoustic pulses (frequencies more than 30 Hz) from the smaller-scale layered structures in the stably-stratified ABL (compared with their scales in the upper atmosphere). Indeed, the vertical profiles of the fine-scale fluctuations of *Ceff*(z) retrieved in the ABL have had vertical scales from 1 to 30 m. (Chunchuzov et al. 2017). Such scales are comparable to the characteristic wavelengths (5–6 m) of acoustic signals generated by the detonation source. On the other hand, the growing with height vertical scales of the fine-scale structures are in the range 100 m–3 km for the upper stratosphere, whereas infrasound signals with periods 0.5–1 Hz have characteristic wavelengths of a few hundred meters, which are also

comparable with the vertical scales of fine-scale structures in the stratosphere.

One of the signals recorded at a distance r = 2.25 km from the anti-hail acoustic cannon (in Fig. 6, bottom) is shown in Fig. 8a. This signal is composed of the arrival propagating in the near-surface waveguide, and the arrivals 1, 2 and 3, detected at the "tail" of the signal using the correlation analysis of signals at the triangular antenna of receivers. The technique for reconstructing the vertical profiles of the fluctuations of the effective sound speed *Ceff* (z) and wind speed from the wave forms and travel times of the reflected signals from the thin inhomogeneous layers in a stably stratified ABL was proposed in (Chunchuzov et al. 2017). The reconstructed profiles of the fluctuations of *Ceff* (z) in these layers with high vertical resolution (of the order of 1 m) are shown in Fig. 8b.

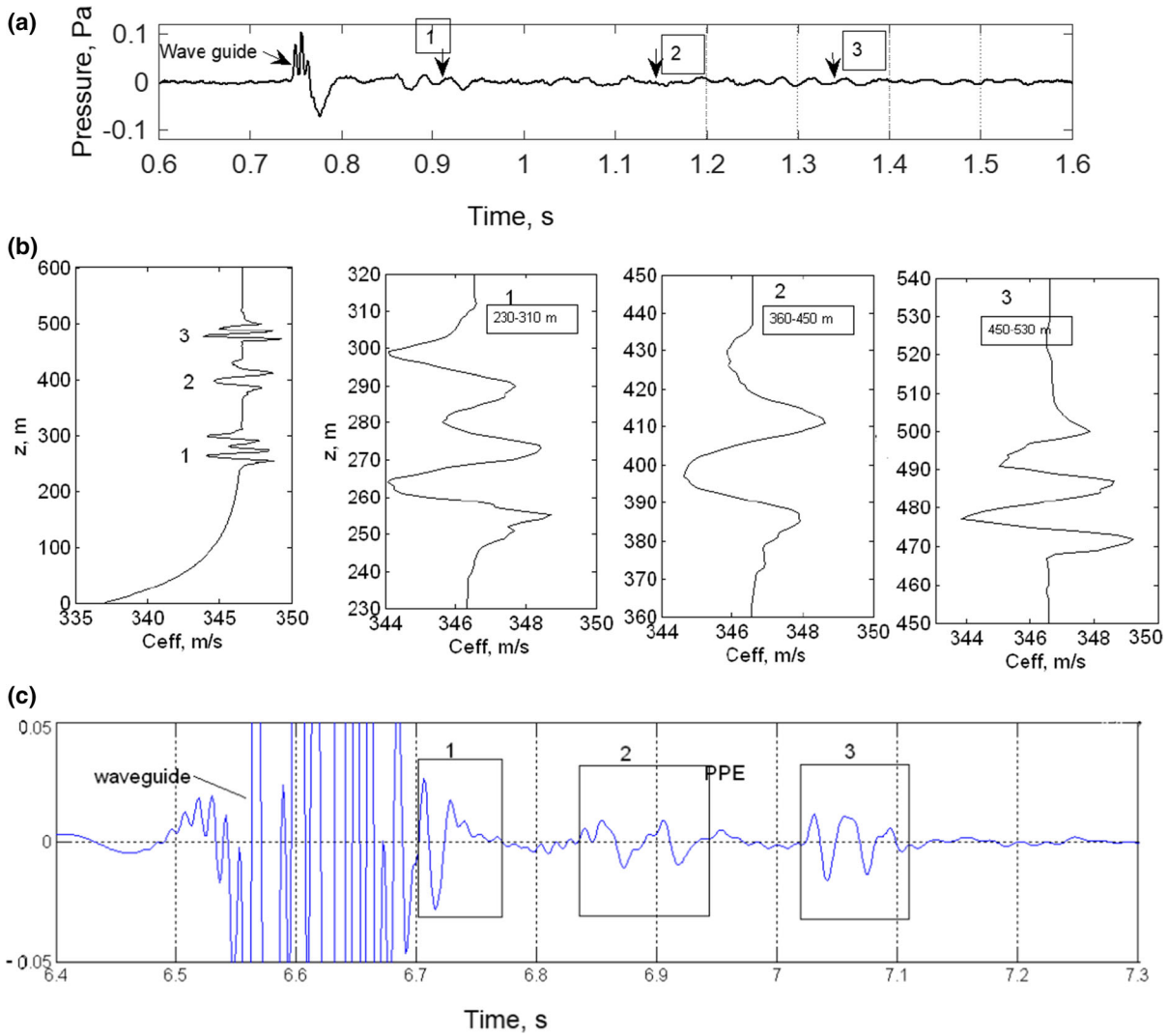

Figure 8

One of the signals recorded at a distance r = 2.25 km from the pulsed source (anti-hail acoustic cannon) and retrieved vertical profiles of the fine-scale layered inhomogeneities of *Ceff* that scatter acoustic pulses in to the shadow zone. The top panel shows the waveguiding arrival, and the arrivals 1, 2 and 3, detected at the "tail" of the signal by using the correlation analysis of signals at the triangular antenna (**a**). Vertical profiles of the fluctuations *Ceff* (z) retrieved from the wave forms and travel times of the arrivals 1, 2 and 3 (**b**). Calculation of the signal by the pseudo-differential parabolic equation (PPE) method for the exponential profile *Ceff* (z) with the retrieved fluctuations in atmospheric layers 1, 2 and 3 (**c**)

The signal calculated by the pseudo-differential parabolic equation (PPE) method for the exponential profile *Ceff* (z) perturbed by the retrieved vertical fluctuations in the atmospheric layers 1, 2, and 3 is shown in Fig. 8c. The amplitudes of the scattered signals 1, 2, and 3 are small compared to the amplitude of the signal that propagates horizontally in the surface acoustic waveguide (indicated as "waveguide" in Fig. 8c). Nevertheless, the appearance in the calculated acoustic field of the scattered signals 1, 2, and 3 is due to the presence of the *Ceff* (z) fluctuations with large vertical gradients, of the order of 0.1–0.3 (m/s)/m, found at different altitudes of the ABL.

Similarly, the vertical profiles of the fluctuations of *Ceff* (z) were retrieved from the arrivals of the acoustic signals generated by the detonation source near Zvenigorod (Fig. 9a) (Chunchuzov et al. 2017). The average (over measurement period) profile of *Ceff* (z) was obtained from the sodar and temperature profiler data. This profile, being superimposed by the retrieved fluctuations of *Ceff* at altitudes of 340–390 m and 560–630 m, is shown in Fig. 9a.

Earlier, a new method of probing of a fine-scale wind layered structure in the stratosphere, mesosphere and lower stratosphere using infrasound from surface explosions and volcanoes was developed in (Chunchuzov et al. 2015a, b). With this method the instant vertical profiles of *Ceff* -fluctuations (designated as D*Ceff*) were retrieved up to altitudes of the lower thermosphere (130 km) at different sites of the globe and at different time periods.

One of the profiles of D*Ceff* fluctuations in the stratosphere, retrieved from the signal recorded on June 2, 2011 in the acoustic shadow zone at a distance of 322 km from the 30 t TNT surface explosion near Izhevsk (Russia,), is shown in Fig. 9b (on the right). The fluctuations are normalized by their standard deviation, whereas height is normalized by the characteristic vertical period of the fluctuations L_V found from their vertical wave number spectra (Chunchuzov et al. 2015b). In the stratospheric layer between 44 and 54 km the vertical scale $L_V \sim 1$ km and std(D*Ceff*) $\sim$ 3.5 m/s.

For comparison, we also normalized the retrieved fluctuations D*Ceff* in the stably stratified ABL between heights of 560 and 640 m (Fig. 9a) by std(D*Ceff*) = 0.7 m/s, and the height z was normalized by characteristic vertical period $L_V \sim 10$ m. In the dimensionless co-ordinates presented here the amplitudes and characteristic periods of the fluctuations in Fig. 9a, b are close to each other, so one can't distinguish of whether the fluctuations of D*Ceff* were retrieved in the stratosphere or in the ABL. Thus, we can model the effect of scattering of infrasound from the fine-scale layered structure of the stratosphere by studying the scattering of acoustic pulses (radiated by detonation generators) from the fine-scale layered structure in stably stratified ABL. Such a modeling in the ABL is possible only up to a certain extent, because it does not take into account the growing with height influence of nonlinear effects on signals from explosions, which leads to the transformation of these signals into an N-wave with two shock fronts at heights of the stratosphere and lower thermosphere (Green et al. 2018). The detonation generators radiate signals in the ABL with only one shock front, and the influence of nonlinear effects on such signals is manifested only up to distances of 100 m from the source. The difference in the forms of signals from the different pulsed sources in the ABL and the upper atmosphere was taken into account by Chunchuzov et al (2017) when finding the relation between the waveform of the scattered signal and the vertical profile of the fluctuations *DCeff* in the ABL.

6. Conclusions

The paper shows the possibility for physical modeling of the long-range propagation of infrasound signals from explosions of different power in the atmosphere by studying the propagation of acoustic pulses from man-made detonation sources in stably stratified ABL. Analyzing the normal mode solution for the acoustic field in the Epstein or exponential atmospheric layers we found that the wave form of the acoustic signal depends on the effective thickness of the wave guide M_m and the distance from the point source normalized to the minimum spatial period of interference of modes. These parameters in the ABL were estimated from the Doppler sodar and temperature profiler measurements.

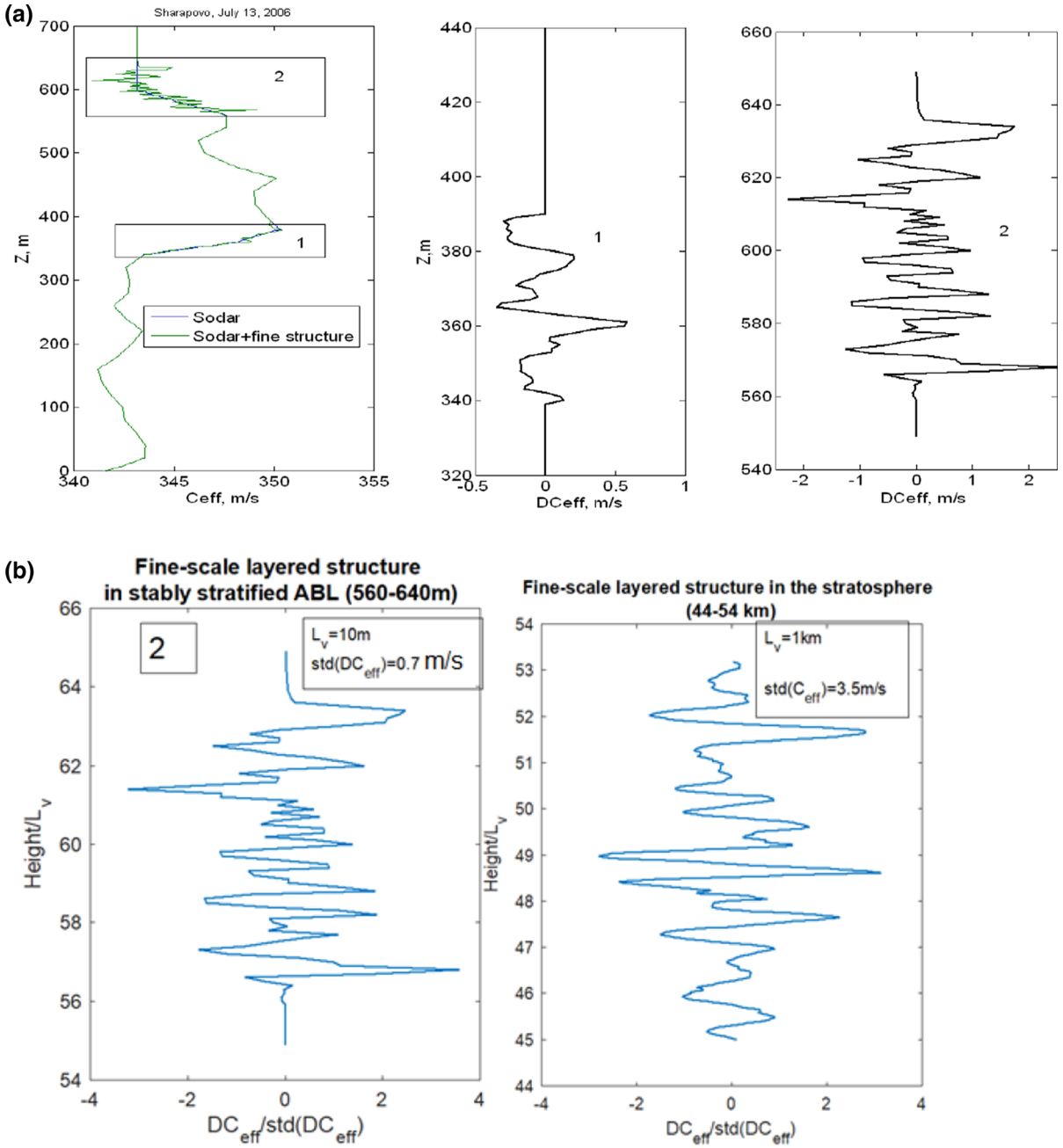

Figure 9

The vertical profile of the effective sound speed obtained from sodar and temperature profiler data with the retrieved vertical fluctuations *Ceff* (*z*) in the layers 1 and 2 (shown on an enlarged scale), which scattered acoustic pulses to the ground (**a**). Comparison of the normalized retrieved fluctuations D*Ceff* (*z*) in stably stratified ABL (bottom left panel) and in the stratosphere (bottom, right panel)

We also found the resemblance between the propagation of the infrasound signals from surface explosions (20–70 t TNT) in the ''shallow'' tropospheric wave guide with $M_m << 1$ and propagation of Lamb mode from nuclear explosions. In the opposite case of "deep" wave guide with $M_m >> 1$ we also modeled (using ray tracing method) the propagation of infrasound signals from surface

explosions in the stratospheric wave guides by studying the propagation of acoustic pulses in the ABL during morning hours (after sunrise), when the convection under the elevated inversion layer shapes an effective sound speed profile similar to that in the stratospheric wave guide.

The effect of scattering of acoustic pulses from a fine-scale layered structures in stably stratified ABL was studied as well. This effect as shown resembles the scattering of infrasound signals from gravity wave perturbations and coherent structures in the upper atmosphere.

Acknowledgements

This work was supported by the RFBR Grants No. 18–55-05002 (Sects. 1, 2, 4, 5) and 18-05-00576 (Sect. 3)

References

Blom, P., & Waxler, R. (2012). Impulse propagation in the nocturnal boundary layer: Analysis of the geometric component. *Journal of the Acoustical Society of America*. https://doi.org/10.1121/1.3699174.

Brekhovskikh, L. M., & Lysanov, Y. P. (2003). *Fundamentals of ocean acoustics*. New York: Springer.

Chunchuzov, I. P. (1986). Evaluation of the nonlinear effects in the propagation of an acoustic pulse in the surface layer of the atmosphere under inversion conditions. *Izvestiya, Atmospheric and Oceanic Physics, 22*(2), 114–119.

Chunchuzov, I. P. (2004). Influence of internal gravity waves on sound propagation in the lower atmosphere. *Meteorology and Atmospheric Physics, 85*(1), 61–76.

Chunchuzov, I. P., Bush, G. A., & Kulichkov, S. N. (1990). On acoustical impulse propagation in a moving inhomogeneous atmospheric layer. *Journal of the Acoustical Society of America, 88*(1), 455–466.

Chunchuzov, I. P., Kulichkov, S. N., Popov, O. E., & Perepelkin, V. G. (2010). The propagation of an acoustic pulse in a near-ground atmospheric waveguide. *Izvestiya, Atmospheric and Oceanic Physics, 46*(5), 597–607.

Chunchuzov, I. P., Kulichkov, S. N., Popov, O. E., Perepelkin, V. G., Vasil'ev, A. P., Glushkov, A. I., et al. (2015a). Characteristics of a fine vertical wind field structure in the stratosphere and lower thermosphere according to infrasonic signals in the zone of acoustic shadow. *Izvestiya, Atmospheric and Oceanic Physics, 51*(1), 57–74.

Chunchuzov, I., Kulichkov, S., Perepelkin, V., Popov, O., Firstov, P., Assink, J. D., et al. (2015b). Study of the wind velocity-layered structure in the stratosphere, mesosphere and lower thermosphere by using infrasound probing of the atmosphere. *Journal of Geophysical Research*. https://doi.org/10.1002/2015JD023276.

Chunchuzov, I. P., Perepelkin, V. G., Popov, O. E., Kulichkov, S. N., Vardayan, A. A., Ayvazyan, G. Y., et al. (2017). Studying characteristics of a fine layered structure of the lower troposphere on the basis of acoustic pulse sounding. *Izvestiya, Atmospheric and Oceanic Physics, 53*(3), 279–293.

Chunchuzov I., Kulichkov, S., Popov, O., Perepelkin, V., Vardanyan, A., & Ayvazyan, G. (2019). Atmospheric boundary layer as a laboratory for modeling infrasound propagation and scattering in the atmosphere. In *Presentation*, *CTBTO science and technology conference* (SnT'19), Vienna, 24–28 June 2019.

Damiens, F., Millet, C., & Lott, F. (2018). An investigation of infrasound propagation over mountain ranges. *Journal of the Acoustical Society of America, 143*(1), 563–574.

Dorfman, A. A., Pelinovskii, E. N., & Stepanyants, Y u A. (1981). Finite-amplitude cylindrical and spherical waves in weakly dispersive media. *Journal of Applied Mechanics and Technical Physics, 22*(2), 206–211.

Drob, D. P., Broutman, D., Hedlin, M. A., Winslow, N. W., & Gibson, R. G. (2013). A method for specifying atmospheric gravity wavefields for long-range infrasound propagation calculations. *Journal of Geophysical Research: Atmospheres, 118*, 3933–3943. https://doi.org/10.1029/2012JD018.

Fritts, D. C., & Alexander, M. J. (2003). Gravity wave dynamics and effects in the middle atmosphere. *Reviews of Geophysics, 41*(1), 1003–2003. https://doi.org/10.1029/2001RG000106.

Gainville, O., Blank-Benon, P., Blanc, E., Roche, R., Millet, C., Le Piver, F., et al. (2010). Misty picture: A unique experiment for the interpretation of the infrasound from large explosive sources. In A. Le Pichon, E. Blanc, & A. Hauchecorne (Eds.), *Infrasound monitoring for atmospheric studies* (pp. 575–598). New York: Springer.

Gibson R., Drob, D., & Broutman, D. (2009). Advancement of techniques for modeling the effects of fine-scale atmospheric inhomogeneities on infrasound propagation. In *Proc. of the 2009 monitoring research review—Ground-based nuclear explosion monitoring technologies*, LA-UR-09–05276 (Vol. 2, pp. 714–723).

Godin, O. A., Mikhin, D. Y., & Molchanov, S. Y. (1993). Effective sound speed approximation in the acoustics of moving media. *Izvestiya, Atmospheric and Oceanic Physics, 29*(2), 179–186.

Green, D. N., Waxler, R., Lalande, J. M., Velea, D., & Talmadge, C. (2018). Regional infrasound generated by the Humming Roadrunner ground truth experiment. *Geophysical Journal International, 214*(3), 1847–1864.

Hedlin, M. A. H., & Walker, K. T. (2013). A study of infrasonic anisotropy and multipathing in the atmosphere using seismic networks. *Philosophical Transactions of the Royal Society A, 371*(1984), 20110542. https://doi.org/10.1098/rsta.2011.0542.

Karpman, V. I. (1974). *Non-linear waves in dispersive media (Nyelineyniye volny v dispergirujushchikh sryedakh). Translated by F. F. Cap* (p. 186). Oxford: Pergamon Press.

Ko, K., & Kuehl, H. H. (1979). Cylindrical and spherical Korteveg-de Vries solitary waves. *Physics of Fluids, 22*(7), 1343–1349.

Kulichkov, S. N. (1987). Propagation of Lamb waves in the atmosphere along the earth's surface. *Izvestiya, Atmospheric and Oceanic Physics, 23*, 1251–1262.

Kulichkov, S. N. (1992). Long-range propagation of sound in the atmosphere (review). *Izvestiya Akademii Nauk SSSR, Fizika Atmosfery Okeana, 28*, 3–20.

Kulichkov, S. N., Chunchuzov, I. P., & Shurygin, E. A. (1986). On sound pulse propagation in the atmospheric wave guide. *Izvestiya, Atmospheric and Oceanic Physics, 21*(2), 131–138.

Kulichkov, S. N., Chunchuzov, I. P., Popov, O. E., Perepelkin, V. G., Svertilov, A. I., Baryshnikov, A. K. (2007). Physical simulation of long-range infrasonic propagation in the atmosphere. In *Inframatics*, No. 19, Sept. 2007, 1–3.

Lalande, J.-M., & Waxler, R. (2016). On the interaction between infrasonic waves and internal gravity waves perturbations: Application to observations using UTTR rocket motor fuel elimination events. *Journal of Geophysical Research: Atmospheres, 121*(10), 5091–6129.

Le Pichon, A., Vergoz, J., Cansi, Y., Geranna, L., & Drob, D. (2010). Contribution of infrasound monitoring for atmospheric remote sensing. In A. Le Pichon, E. Blanc, & A. Hauchecorne (Eds.), *The book: Infrasound monitoring for atmospheric studies* (pp. 629–646). New York: Springer.

Millet, C., et al. (2019). Learning about small-scale atmospheric structures through recurrent infrasound events. In *Abstract. CTBTO science and technology conference (SnT 2019)*, June 2019, Hofburg, Vienna. https://ctnw.ctbto.org/ctnw/abstract/32887**.**

Ostashev, V. E., & Wilson, D. K. (2015). *Acoustics in moving inhomogeneous media* (2nd ed.). Boca Raton: CRC Press.

Pelinovskii, E. N. (1982). *Nelineinaya dinamika voln tsunami (Nonlinear Dynamics of Tsunamis)*. Izd: Inst. Prikladn. Fiz. AN SSSR, Gor'kii. **(in Russian)**.

Pelinovskiy, E. N., Fridman, V. E., & Engel'brekht, Y. K. (1984). *Nonlinear equations of evolution*. Tallinn: Valgus.

Pierce, A. D., & Posey, J. W. (1971). Theory of the excitation and propagation of lamb's atmospheric edge mode from nuclear explosions. *Geophysical Journal International, 26*(1–4), 341–368. https://doi.org/10.1111/j.1365-246X.1971.tb03406.x.

Sabatini, R., Marsden, O., Bailly, C., & Gainville, O. (2019). Three-dimensional direct numerical simulation of infrasound propagation in the Earth's atmosphere. *Journal of Fluid Mechanics, 859*, 754–789.

Talmadge, C. L., Waxler, R., XiaoGilbert, D. K., & Kulichkov, S. (2008). Observation of low-frequency acoustic surface waves in the nocturnal boundary layer. *Journal of the Acoustical Society of America, 124*(4), 1956–1962.

Waxler, R. (2002). A vertical eigenfunction expansion for the propagation of sound in a downward-refracting atmosphere over a complex impedance plane. *Journal of the Acoustical Society of America, 112*(6), 2540–2552.

Waxler, R., & Assink, J. (2019). Propagation modeling through realistic atmosphere and benchmarking: Challenges in middle atmosphere dynamics and societal benefits. In A. Le Pichon, E. Blanc, & A. Hauchecorne (Eds.), *Chapter 15: Infrasound monitoring for atmospheric studies* (pp. 509–549). New York: Springer. https://doi.org/10.1007/978-3-319-75140-5_16

Waxler, R., Gilbert, K. E., & Talmadge, C. (2008). A theoretical treatment of the long range propagation of impulsive signals under strongly ducted nocturnal conditions. *Journal of the Acoustical Society of America, 124*(5), 2742–2754.

Zakharov, V. E., Manakov, S. V., Novikov, S. P., & Pitaevskii, L. P. (1980). *Soliton theory inverse scattering method*. Moscow: Nauka.

(Received September 29, 2019, revised May 5, 2020, accepted May 8, 2020)